RSC Advances

PAPER

View Article Online
View Journal | View Issue

Cite this: *RSC Adv.*, 2018, **8**, 8118

Electrolytic extraction of dysprosium and thermodynamic evaluation of Cu–Dy intermetallic compound in eutectic LiCl–KCl

Wei Han,[*ab] Zhuyao Li,[a] Mei Li,[*ab] Yinyi Gao,[ab] Xiaoguang Yang,[ab] Milin Zhang[ab] and Yang Sun[ab]

The electrochemical reduction of dysprosium(III) was studied on W and Cu electrodes in eutectic LiCl–KCl by transient electrochemical methods. Cyclic voltammogram and current reversal chronopotentiogram results demonstrated that dysprosium(III) was directly reduced to dysprosium (0) on the W electrode through a single-step process with the transfer of three electrons. Electrochemical measurements on the Cu electrode showed that different Cu–Dy intermetallics are formed. Moreover, the thermodynamic properties of Cu–Dy intermetallic compounds were estimated by open circuit chronopotentiometry in a temperature range of 773–863 K. Using the linear polarization method, the exchange current density (j_0) of dysprosium in eutectic LiCl–KCl on the Cu electrode was estimated, and the temperature dependence of j_0 was studied to estimate the activation energies associated with Dy(III)/Cu_5Dy and Dy(III)/$Cu_{9/2}Dy$ couples. In addition, potentiostatic electrolysis was conducted to extract dysprosium on the Cu electrode, and five Cu–Dy intermetallic compounds, CuDy, Cu_2Dy, $Cu_{9/2}Dy$, Cu_5Dy and $Cu_{0.99}Dy_{0.01}$ were identified by X-ray diffraction, scanning electron microscopy and energy dispersive spectrometry. Meanwhile, the change of dysprosium(III) concentration was monitored using inductively coupled plasma-atomic emission spectrometry, and the maximum extraction efficiency of dysprosium was found to reach 99.2%.

Received 18th December 2017
Accepted 5th February 2018

DOI: 10.1039/c7ra13423a

rsc.li/rsc-advances

Introduction

Nowadays, nuclear energy is regarded as a prospective energy source for the future generation and attracts much attention due to being clean and having a high energy density. However, how to effectively manage the spent nuclear fuels in a safe and economic manner has become one of the most important problems related to the sustainable development of nuclear energy productions. Pyrometallurgical techniques, giving a drastic reduction in radioactive waste, engineering support of the fissile material nonproliferation principle and lowering of the amount reprocessing required of spent nuclear fuels,[1] are a promising alternative to hydrometallurgical techniques for the recovery of actinides from spent fuels.[2,3] The electrochemical deposition on the solid or liquid electrode in molten salts[4–6] or molten salts–liquid metal reductive extraction[7,8] are the most developed pyrochemical methods designed for the separation of actinides from fission products in molten chlorides and fluoride salts.

Lanthanides are often used as surrogates because they have similar electrochemical properties to actinides. Thus, electrolytic extraction of lanthanides were carried out in chloride molten salt or fluoride molten salt systems using reactive solid cathodes, such as Al,[9–11] Mg,[12–14] Ni,[15–23] or Cu.[24–26] Taxil *et al.*[24] and Gibilaro *et al.*[27] electrochemically extracted Nd, Gd, Sm and Eu on a Ni cathode in a LiF–CaF_2–LnF_3 (Ln = Nd, Gd, Sm and Eu) molten salt system. Nourry *et al.*[26] investigated the electrolytic extraction of metallic Nd and Gd in LiF–CaF_2 melts on Ni and Cu electrodes, respectively. They found that the extraction rate on the Cu electrode was faster than that on Ni electrode in the temperature of 1113–1193 K. Our research group successfully extracted ytterbium[28] and erbium[29] on a Cu cathode, and found that the extraction efficiencies of ytterbium and erbium on a Cu electrode could reach 99.9% and 98.9%, respectively.

As a typical fission product element, dysprosium should be removed from actinides due to its high thermal neutron absorption cross-section. Therefore, its electrochemical separation and extraction was explored on different electrodes in molten salts. Castrillejo *et al.*[30] researched the electrochemical behavior of dysprosium and formation of Dy–Al alloys on an Al electrode in the eutectic LiCl–KCl. The electrochemical production of Dy–Fe alloy films was explored on a Fe electrode

[a]*Key Laboratory of Superlight Materials and Surface Technology, Ministry of Education, College of Material Science and Chemical Engineering, Harbin Engineering University, Harbin 150001, China. E-mail: weihan@hrbeu.edu.cn; Fax: +86 451 8253 3026; Tel: +86 451 8256 9890*

[b]*Institute of Nuclear Energy and Safety, Harbin Engineering University, Harbin 150001, China*

using a molten salt electrochemical process.[31] Yang *et al.*[13] obtained the Dy–Mg alloys during selective electrochemical deposition of dysprosium on a Mg electrode in LiCl–KCl–$DyCl_3$–$GdCl_3$ molten salts. Since the Dy–Ni intermetallic compounds have a magnetocaloric effect,[32,33] the electrochemical preparation of Dy–Ni intermetallic compounds was explored in molten salts on a Ni electrode[17,19,20,25,34,35] and $DyNi_2$ electrode,[19,34,35] respectively. However, Cu–Dy alloy, as a magnetic material,[36,37] has not been produced by molten salt electrolysis.

Therefore, in order for electrochemical extraction of dysprosium and formation of Cu–Dy alloys, it is necessary to explore the kinetic properties of Dy(III) on the Cu electrode and the thermodynamic properties of formation of Cu–Dy intermetallics. Thus, the electrochemical behavior of Dy(III) was first studied on the Cu electrode in eutectic LiCl–KCl using transient electrochemical techniques, for example, cyclic voltammetry (CV) and square wave voltammetry (SWV). Thermodynamic data of Cu–Dy intermetallics were calculated by open circuit chronopotentiometry (OCP). Meanwhile, the exchange current density (j_0) and activation energy (E_a) for Dy(III) on the Cu electrode were investigated by linear polarization. Then, electrochemical extraction of dysprosium and preparation of Cu–Dy alloy were conducted on the Cu electrode by potentiostatic electrolysis at different electrolytic potentials. Next, the surface morphology and composition of the Cu–Dy alloy were analyzed by SEM-EDS and XRD. Furthermore, the extraction efficiency was estimated by measuring the concentration change of Dy(III) in the melts and mass change of the working electrode.

Experimental

Preparation of melts

A mixture of LiCl–KCl with eutectic composition (45.8 : 54.2 wt%, Anhydrous, AR, Tianjin Kermel Chemical Reagent Co., Ltd.) was dried at 553 K for 24 h to minimize the amount of residual water. Then, in order to remove the impurities in LiCl–KCl melts, pre-electrolysis was performed at −2.1 V (*vs.* Ag^+/Ag) for 4 h. The temperature of the molten salt was measured with a chromel–alumel thermocouple sheathed by an alumina tube. Anhydrous $DyCl_3$ (99.9%; Koya fine chemicals Co., Ltd.) was introduced into the eutectic melts as the Dy(III) ions source. Moreover, to prevent the materials from reacting with oxygen or water vapor, all chemicals were operated under a high purity argon atmosphere.

Electrode and electrochemical device

The transient electrochemical techniques (CV, SWV and CP) and steady state technique (OCP) were conducted in an electrochemical cell with a three electrode set-up. All electrochemical studies were performed with the Metrohm Electrochemical Workstation (AUTOLAB PGSTAT302N) with electrochemical software (NOVA 1.10). The reference electrode is comprised of a silver wire of 1 mm in diameter dipped into a AgCl solution (1 wt%) in eutectic LiCl–KCl, contained in a Pyrex tube. All potentials in this work were referenced to the Ag/AgCl reference electrode. The auxiliary electrode was a graphite rod (Ø 6.0 mm) of spectral purity. Tungsten wire of 1 mm (99.99%) in diameter, or Cu wire (99.99%; Wantong Metal material Co., Lot; $S = 0.72$ cm^2) or Cu plate (99.99%; Wantong Metal material Co., Lot; $S = 2.15$ cm^2) were used as the working electrode. The surface of the working electrode was polished with SiC paper and then washed with distilled water and alcohol, respectively.

Characterization of extracting products and determination of Dy(III) concentration

The electrochemical extraction of dysprosium was conducted on the Cu electrode by potentiostatic electrolysis, and then the extractive Cu–Dy alloy was washed with distilled water and absolute ethyl alcohol (99.7%) to remove the solidified salts attached to its surfaces. After that, the composition, morphology and micro-zone chemical analysis of extractive products were characterized by X-ray diffraction (XRD, Philips, Netherlands) and scanning electron microscope and energy dispersive spectrometer (SEM-EDS, HITACHI SU-70, Japan). The mass change of the working electrode was weighed using an electronic balance (Denver Instrument, TB-215D, $d_{60\ g} = 1 \times 10^{-5}$ g). In order to monitor the change of Dy(III) ions concentration during the electrochemical extraction of dysprosium, a salt sample was taken out from the molten salts at various electrolysis times, and then dissolved in ultrapure water. After that, Dy(III) ions concentration in the eutectic melts was analyzed by inductively coupled plasma-atomic emission spectrometry (ICP-AES, Thermo Elemental, IRIS Intrepid II XSP) and the extraction efficiency was evaluated.

Results and discussion

Electrochemical reduction of Dy(III) ions on the W electrode

CV is a common electrochemical technology for investigating the electrode process and reaction mechanism, thus, it was adopted in this section to investigate the redox process of Dy(III)/Dy on the tungsten electrode in eutectic LiCl–KCl.

Fig. 1 presents the typical cyclic voltammograms attained in eutectic LiCl–KCl before and after the addition of $DyCl_3$ on the tungsten electrode at 773 K. The black curve represents a typical cyclic voltammogram of the eutectic LiCl–KCl. It can be seen that only one pair of redox electrical signals I/I′, observed at about of −2.39 V/−2.20 V (*vs.* Ag/AgCl), is ascribed to the deposition and re-dissolution of lithium metal.

The red curve shows the cyclic voltammogram of $DyCl_3$ (1.34×10^{-4} mol cm^{-3}) in eutectic LiCl–KCl. In addition to the pair of signals I/I′ mentioned above, a pair of new redox signals II/II′ is detected at approximately −2.01 V/−1.83 V (*vs.* Ag/AgCl), which are related to the reduction re-oxidation of dysprosium. No other peak signal, apart from electrical signals II/II', are found before that of the deposition of metallic lithium, suggesting that the reduction of Dy(III) is a one-step process without a co-deposition reaction of Li(I) and Dy(III) ions. The results agree with those reported by Sridharan *et al.*[38] and Shi *et al.*[39]

Current reversal chronopotentiogram of $DyCl_3$ in LiCl–KCl melts was recorded at $I = \pm 15$ mA, as shown in Fig. 1. The

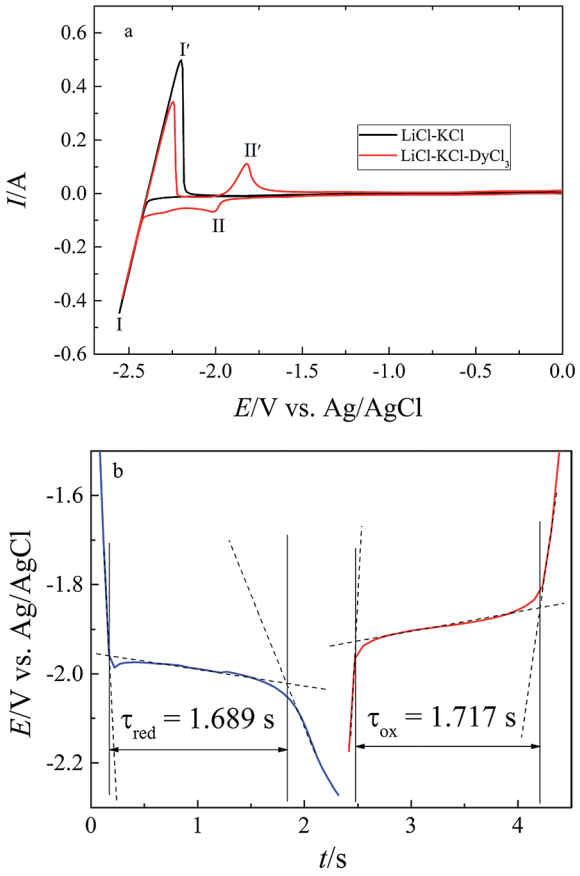

Fig. 1 (a) Cyclic voltammograms attained on the W electrode in the absence and presence of $DyCl_3$ in eutectic LiCl–KCl; (b) current reversal chronopotentiogram attained on the W electrode in molten LiCl–KCl–$DyCl_3$ (1.34×10^{-4} mol cm^{-3}) salts. Cathodic current: −15 mA; anodic current: 15 mA; *T*: 773 K. Electrode area: 0.345 cm^2.

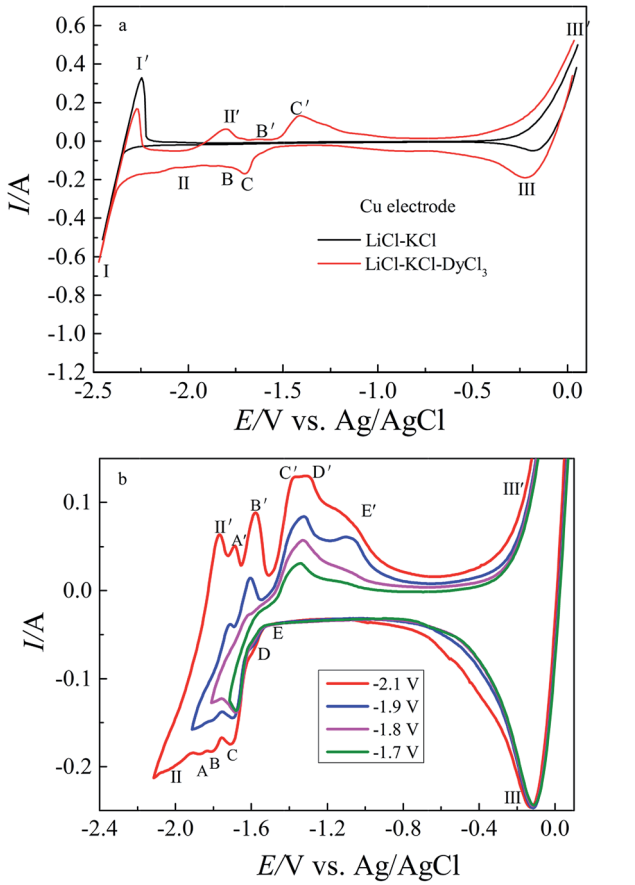

Fig. 2 (a) Cyclic voltammograms of blank eutectic LiCl–KCl (black line) and molten LiCl–KCl–$DyCl_3$ salts (red line); (b) cyclic voltammograms of molten LiCl–KCl$DyCl_3$ salts at various inversion potentials. Working electrode: Cu; electrode area: 0.72 cm^2; *T*: 773 K; scan rate: 0.1 V s^{-1}.

transit times (τ_{ed} and τ_{ox}) of the two potential plateaus (−1.99 V and −1.88 V) are approximately equal, this demonstrates that electrochemical reduction of the Dy(III) process is one-step and forms insoluble metallic Dy.

$$Dy(III) + 3e^- = Dy(0) \quad (1)$$

Electrochemical reduction of Dy(III) ions on the Cu electrode

Research results of CV and SWV. The comparison of cyclic voltammograms is presented in Fig. 2a, obtained in eutectic LiCl–KCl (black curve) and LiCl–KCl–$DyCl_3$ (1.34×10^{-4} mol cm^{-3}, red curve) melts. It can be seen from the black curve that two couples of cathodic/anodic signals are observed. Except for the cathodic/anodic signals I/I′ corresponding to the reduction/re-oxidation of metallic lithium, a new pair of signals III/III′ is observed. The cathodic signal III at about −0.27 V and the corresponding anodic peak III′ at about −0.11 V in the reverse scan direction are ascribed to the deposition and dissolution of Cu metal, which is found to be in line with our previous experimental results.[28,29] After the addition of $DyCl_3$ (1.34×10^{-4} mol cm^{-3}) into the eutectic melts, a series of cathodic/anodic signals were observed from the red curve. In addition to the cathodic/anodic signals I/I′ and III/III′ mentioned above, the signals II/II′, located at −1.98 V/−1.82 V, are related to the reduction/re-oxidation of metallic Dy. While the other cathodic and their corresponding anodic signals, between signals II/II′ and III/III′, should be related to the formation/re-dissolution of different Cu–Dy intermetallic compounds. Since deposited Dy reacts with Cu metal to form Cu–Dy intermetallics, the reduction potential of the Dy(III)/Dy(0) couple is detected at less negative potential values than that on the W electrode. The formation of Cu–Dy intemetallic compounds is described as follows:

$$Dy(III) + 3e^- + xCu = Cu_xDy \quad (2)$$

For confirming the attribution of these redox peaks, the cyclic voltammograms were registered at different reversion potentials as shown in Fig. 2b. It is obvious that five pairs of redox signals, A/A′, B/B′, C/C′, D/D′ and E/E′ observed at −1.86 V/−1.67 V, −1.80 V/−1.57 V, −1.71 V/−1.37 V, −1.58 V/−1.28 V and −1.45/−1.08 V, are correlated with the formation and dissolution of five Cu–Dy intermetallics. Based on the phase

diagram of the Cu–Dy binary system,[40,41] there are four thermodynamically stable Cu–Dy intermetallics (CuDy, Cu_2Dy, $Cu_{9/2}Dy$ and Cu_5Dy). Thus, we suggested that the thermodynamically metastable phase might form under such conditions.

Fig. 3 shows the SWV recorded on the Cu electrode in molten LiCl–KCl–$DyCl_3$ (1.34×10^{-4} mol cm^{-3}) salts at various frequencies. It is clear that these cathodic peak currents increase with the increase of frequency. As seen from Fig. 3, there are eight reductive peaks observed in the electrochemical window. Based on the results shown in Fig. 2, the attribution of eight reduction signals could be confirmed. Three reduction peaks I, II and III, detected at −2.40 V, −2.04 V and −0.24 V, respectively, are ascribed to the deposition of metallic Li, Dy and Cu, respectively. The other five reduction current peaks A, B, C, D and E observed at −1.88 V, −1.79 V, −1.68 V, −1.59 V and −1.44 V, respectively, are ascribed to the deposition of metallic Dy on the Cu electrode to form five different Cu–Dy intermetallic compounds. Comparison of the reduction peak potentials obtained by CV and SWV are presented in Table 1. It can be seen from Table 1 that the results gained by CV are consistent with those obtained by SWV.

Research results of OCP. As a steady state technique, OCP is commonly used to obtain the equilibrium potential of formation for different intermetallics. Therefore, OCP was employed on the Cu electrode in molten LiCl–KCl–$DyCl_3$ salts at different temperatures. The measurement was conducted as follows: after a short cathodic polarization at −2.5 V (*vs.* Ag/AgCl) for 50 s at 773 K, metallic Dy was firstly electrodeposited on the Cu electrode. After stopping the polarization, the Cu electrode was kept in the melts. During the currentless process, the open circuit potential was registered *vs.* time. A series of potential plateaus occur in the open circuit chronopotentiogram and each potential plateau is related to a two-phase coexistence state on the Cu electrode surface.

Fig. 4a (black curve) shows the open circuit chronopotentiogram detected on the Cu electrode after a short cathodic polarization at −2.5 V (Ag/AgCl) for 80 s in molten LiCl–KCl–$DyCl_3$ (1.34×10^{-4} mol cm^{-3}) salts at 773 K. It can be seen that there are seven potential plateaus in the black curve. To confirm the ascription of the potential plateau, the open circuit chronopotentiograms of eutectic LiCl–KCl (blue curve) on the Cu electrode and molten LiCl–KCl–$DyCl_3$ salt (red curve) on the W electrode are also presented in Fig. 4a after potentiostatic electrolysis at −2.5 V for 80 s. Based on the results of CV and SWV (shown in Fig. 2 and 3), the first plateau I occurs near −2.42 V interpreted due to the formation of metallic Li on the Cu electrode and correlated with the redox couple of Li(I)/Li(0).

The second plateau II observed at about −1.90 V is related to the equilibrium of the Dy(III)/Dy(0) redox couple. After that,

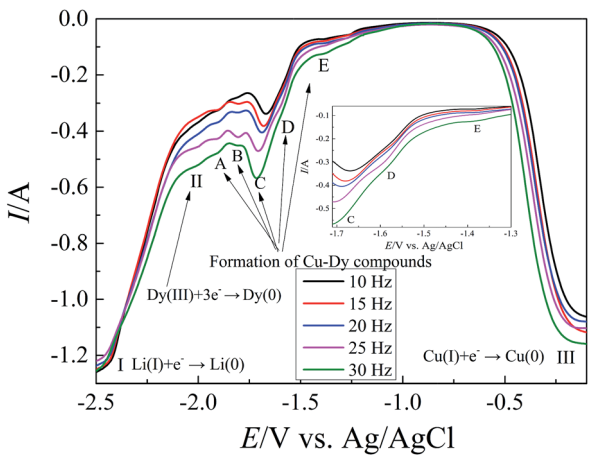

Fig. 3 Square wave voltammograms attained in molten LiCl–KCl–$DyCl_3$ (1.34×10^{-4} mol cm^{-3}) salts on a Cu electrode ($S = 0.72$ cm^2) at 773 K. Potential step: 1 mV; frequency: 10–30 Hz.

Table 1 Summary of the peak potentials obtained by different electrochemical techniques

Electrochemical techniques	Reduction peak potentials/V						
	II	A	B	C	D	E	III
CV	−2.02	−1.86	−1.80	−1.71	−1.58	−1.45	−0.11
20 Hz SWV	−2.00	−1.88	−1.79	−1.68	−1.59	−1.44	−0.14

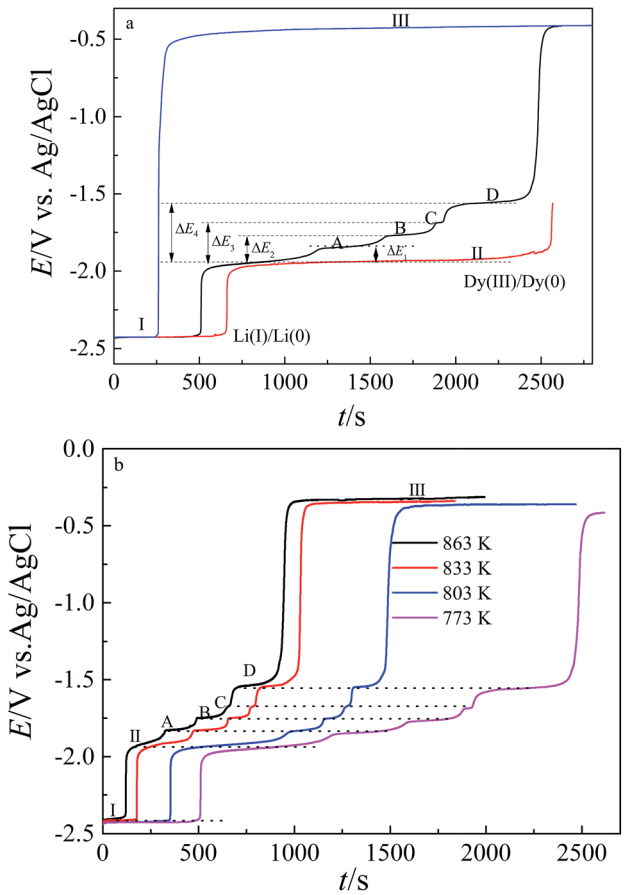

Fig. 4 (a) Open circuit chronopotentiograms recorded in molten LiCl–KCl–$DyCl_3$ (red line) salts on W electrode ($S = 0.345$ cm^2), eutectic LiCl–KCl (blue line) and molten LiCl–KCl–$DyCl_3$ (black line) salts on a Cu electrode ($S = 0.72$ cm^2) at 773 K and (b) open circuit chronopotentiograms recorded on Cu electrode ($S = 0.72$ cm^2) in molten LiCl–KCl–$DyCl_3$ salts at different temperature. Deposition potential: −2.5 V; time: 80 s.

Table 2 Thermodynamic properties of Dy for Cu–Dy intermetallic compounds in two-phase coexisting states at different temperatures

T/K	E_{eq}/V *vs.* Ag/AgCl	ΔE/V *vs.* Dy(III)/Dy	$\Delta\bar{G}_{Dy}$/kJ (mol Dy)$^{-1}$	a_{Dy}
Plateau(Dy)				
773	−1.943 ± 0.003			
803	−1.925 ± 0.005			
833	−1.917 ± 0.002			
863	−1.912 ± 0.002			
Plateau D	In the two-phase coexisting state between Cu_5Dy and Cu			
773	−1.557 ± 0.001	0.386 ± 0.004	−111.75 ± 1.16	2.81×10^{-8}
803	−1.546 ± 0.004	0.379 ± 0.009	−109.72 ± 2.61	7.29×10^{-8}
833	−1.54 ± 0.003	0.377 ± 0.005	−109.14 ± 1.45	1.43×10^{-7}
863	−1.538 ± 0.005	0.374 ± 0.007	−108.27 ± 2.03	2.79×10^{-7}
Plateau C	In the two-phase coexisting state between $Cu_{9/2}Dy$ and Cu_5Dy			
773	−1.686 ± 0.002	0.257 ± 0.005	−74.40 ± 1.45	9.38×10^{-6}
803	−1.678 ± 0.004	0.247 ± 0.009	−71.51 ± 2.61	2.23×10^{-5}
833	−1.675 ± 0.002	0.242 ± 0.004	−70.06 ± 1.61	4.04×10^{-5}
863	−1.671 ± 0.001	0.241 ± 0.003	−69.77 ± 0.87	5.98×10^{-5}
Plateau B	In the two-phase coexisting state between Cu_2Dy and $Cu_{9/2}Dy$			
773	−1.763 ± 0.004	0.18 ± 0.007	−52.11 ± 2.03	3.01×10^{-4}
803	−1.750 ± 0.003	0.175 ± 0.008	−50.66 ± 2.32	5.06×10^{-4}
833	−1.746 ± 0.006	0.171 ± 0.008	−49.51 ± 2.32	7.86×10^{-4}
863	−1.743 ± 0.004	0.169 ± 0.006	−48.93 ± 1.74	1.09×10^{-3}
Plateau A	In the two-phase coexisting state between CuDy and Cu_2Dy			
773	−1.843 ± 0.004	0.1 ± 0.007	−28.95 ± 2.03	1.11×10^{-2}
803	−1.828 ± 0.003	0.097 ± 0.008	−28.08 ± 2.32	1.49×10^{-2}
833	−1.826 ± 0.004	0.091 ± 0.006	−26.35 ± 1.74	2.23×10^{-2}
863	−1.823 ± 0.005	0.089 ± 0.007	−25.77 ± 2.03	2.76×10^{-2}

there are four potential plateaus A, B, C and D. There are four Cu–Dy intermetallics, CuDy, Cu_2Dy, $Cu_{9/2}Dy$ and Cu_5Dy, in the system,[40,41] thus, the four potential plateaus should correlate with the co-existence of two phases of four Cu–Dy intermetallics, respectively. Furthermore, according to the result, we inferred that the reduction signal E in the CV (Fig. 2) and SWV (Fig. 3) is ascribed to the formation of a metastable phase of the Cu–Dy intermetallics. The last potential plateau III observed at about −0.28 V corresponds to the equilibrium of Cu(I)/Cu according to the results reported by Castrillejo *et al.*[42]

Therefore, each potential plateau correlated with the equilibrium reaction can be expressed as follows:

$$\text{Plateau I: Li(I)} + e^- \leftrightarrow \text{Li} \quad (3)$$

$$\text{Plateau II: Dy(III)} + 3e^- \leftrightarrow \text{Dy} \quad (4)$$

$$\text{Plateau D: Dy(III)} + 3e^- + 5\text{Cu} \leftrightarrow \text{Cu}_5\text{Dy} \quad (5)$$

$$\text{Plateau C: Dy(III)} + 3e^- + 9\text{Cu}_5\text{Dy} \leftrightarrow 10\text{Cu}_{9/2}\text{Dy} \quad (6)$$

Table 3 Standard Gibbs free energies of formation for Cu–Dy intermetallic compounds

Intermetallic compound	Formula	T/K	$\Delta G_f^{\ominus}$/kJ mol^{-1}
Cu_5Dy	$\Delta G_f^{\ominus}(Cu_5Dy) = -3F\Delta E_4$	773	−111.75 ± 1.16
		803	−109.72 ± 2.61
		833	−109.14 ± 1.45
		863	−108.27 ± 2.03
$Cu_{9/2}Dy$	$\Delta G_f^{\ominus}(Cu_{9/2}Dy) = \frac{1}{10}[9\Delta G_f^{\ominus}(Cu_5Dy) - 3F\Delta E_3]$	773	−108.01 ± 1.19
		803	−105.89 ± 2.61
		833	−105.23 ± 1.42
		863	−104.42 ± 1.91
Cu_2Dy	$\Delta G_f^{\ominus}(Cu_2Dy) = \frac{5}{9}\left[\frac{4}{5}\Delta G_f^{\ominus}(Cu_{9/2}Dy) - 3F\Delta E_2\right]$	773	−76.96 ± 1.65
		803	−75.21 ± 2.45
		833	−74.27 ± 1.92
		863	−73.59 ± 1.81
CuDy	$\Delta G_f^{\ominus}(CuDy) = \frac{1}{2}[\Delta G_f^{\ominus}(Cu_2Dy) - 3F\Delta E_1]$	773	−52.95 ± 1.84
		803	−51.65 ± 2.38
		833	−50.31 ± 1.83
		863	−49.68 ± 1.92

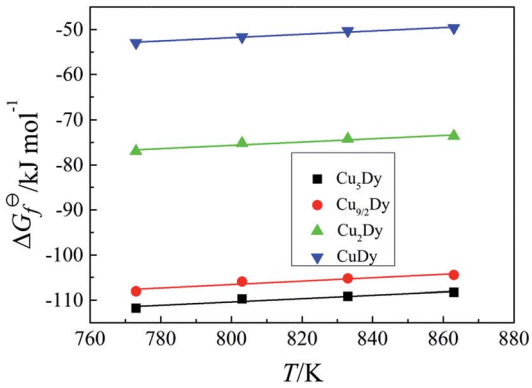

Fig. 5 Change of Gibbs energies of formation for different Cu–Dy intermetallic compounds with temperature.

$$\text{Plateau B}: \mathrm{Dy(III)} + 3e^- + \frac{4}{5}\mathrm{Cu_{9/2}Dy} \leftrightarrow \frac{9}{5}\mathrm{Cu_2Dy} \quad (7)$$

$$\text{Plateau A}: \mathrm{Dy(III)} + 3e^- + \mathrm{Cu_2Dy} \leftrightarrow 2\mathrm{CuDy} \quad (8)$$

Fig. 4b illustrates the open circuit chronopotentiograms recorded in molten LiCl–KCl–$DyCl_3$ salts after potentiostatic deposition at −2.5 V for 80 s at different temperatures. To ensure the reproducibility of the results of the OCP, the measurement was carried out several times under the same conditions. As can be seen from Fig. 4, the plateau length, correlated with the corresponding equilibrium reaction, grows shorter with an increase of temperature at the same conditions, which indicates that the dissolving rate of Cu–Dy intermetallics increases with the increasing of temperature.

The equilibrium potentials in this experiment are referred to the Ag^+/Ag couple, thus, these can be converted to the electromotive forces (emf) against Dy(0). The potential values (ΔE *vs.* Dy(III)/Dy) are obtained at various temperatures and listed in Table 2.

On the basis of the value of ΔE *vs.* (Dy(III)/Dy(0))/V, the activities and the partial molar Gibbs free energy ($\Delta\bar{G}_{Dy}$) of Dy in various Cu–Dy intermetallics are estimated by the following equation:

$$\mathrm{emf} = \Delta E = -(RT/3F)\ln a_{Dy} = -\Delta\bar{G}_{Dy}/3F \quad (9)$$

The calculated results are also presented in Table 2. As can be seen from Table 2, the activity values of Dy in Cu–Dy alloys are in the order of 10^{-8} to 10^{-2}.

When the two phase equilibrium of $CuDy_{x1}$ and $CuDy_{x2}$ exists on the Cu electrode surface, the emf has a constant value during the whole transformation of $CuDy_{x1}$ into the $CuDy_{x2}$. For an intermetallic compound with exact composition, $CuDy_{x2}$ for example, it can be observed that a variation of the emf from the value of the two phase plateau is related to the mixture of $CuDy_{x1}$ and $CuDy_{x2}$ to the value of the two phase plateau of the $CuDy_{x2}$ and $CuDy_{x3}$ mixture. The standard Gibbs energies of formation for an intermetallic compound $CuDy_{x2}$ are related to that of a $CuDy_{x1}$ by the relation:

$$\Delta G_f^{\ominus}(\mathrm{CuDy}_{x2}) = -3F\int_{x1}^{x2}\Delta E(x)\mathrm{d}x + \Delta G_f^{\ominus}(\mathrm{CuDy}_{x1}) \quad (10)$$

The calculated formulas of standard molar Gibbs free energies of formation for different Cu–Dy intermetallic compounds and results are presented in Table 3.

The change of standard molar Gibbs free energy of formation for various Cu–Dy intermetallics with temperature is shown in Fig. 5. The standard molar enthalpies of formation and standard molar entropies, as well as the standard equilibrium constant of formation of each of the Cu–Dy intermetallics are obtained based on the slope of the linear relationship, and the results are listed in Table 4.

Palumbo *et al.*[41] determined the standard mole enthalpy of formation for Cu_5Dy intermetallics by high-temperature direct calorimetry in the temperature range of 298–3000 K. They found the value to be −116.4 kJ mol^{-1}, which is slightly less than our result. Sommer *et al.*[43] measured the standard mole enthalpy of formation for the $Cu_{9/2}Dy$ intermetallic compound by solution calorimetry at 1098 K and the calculated result is −121 ± 2.2 kJ mol^{-1}, which is smaller than our result. The difference may be related to the difference of experimental methods and existence states of the Cu–Dy intermetallic compounds.

Research results of LP. The exchange current density is an important kinetics parameter, related to the nucleation characteristics and morphology of electrodeposits. Thus, the linear polarization (LP) technique was carried out to determine the exchange current density (j_0) of dysprosium on the Cu electrode. At very low overpotentials, the Butler–Volmer equation[44] can be simplified to the following expression:

$$j/\eta = j_0(nF/RT) \quad (11)$$

where j is the net current density, j_0 denotes the exchange current density, and $\eta = E - E_{eq}$ is the overpotential defined

Table 4 Thermodynamic properties of Cu–Dy intermetallic compounds

Intermetallic compound	$\Delta H_f^{\ominus}$/kJ mol^{-1}	$\Delta S_f^{\ominus}$/J mol^{-1} K^{-1}	$\Delta G_f^{\ominus}(T)$/kJ mol^{-1}	$K^{\ominus}$
Cu_5Dy	−139.72 ± 2.14 −116.4 (ref. 41)	−36.67 ± 0.0048	−139.72 + 0.036T	exp(−4.33 + 1685/T)
$Cu_{9/2}Dy$	−137.07 ± 0.43 −121 ± 2.2 (ref. 43)	−38.12 ± 0.0016	−137.07 + 0.038T	exp(−4.57 + 16 486/T)
Cu_2Dy	−105.09 ± 2.09	−36.78 ± 0.0002	−105.09 + 0.036T	exp(−4.33 + 12 641/T)
CuDy	−81.58 ± 2.84	−37.21 ± 0.001	−81.58 + 0.037T	exp(−4.45 + 9813/T)

with respect to a specific reaction. In this study, the exchange current densities were determined for Dy(III)/Cu_5Dy and Dy(III)/$Cu_{9/2}Dy$ couples by the LP technique.

Fig. 6 shows the cathodic polarization curves obtained at the equilibrium potential of Dy(III)/Cu_5Dy and Dy(III)/$Cu_{9/2}Dy$ couples, respectively, in LiCl–KCl–$DyCl_3$ melts on the Cu electrode at a scan rate of 2 mV s^{-1} and ±15 mV (Fig. 6a) and ±13 mV (Fig. 6b) overpotentials. According to the slope of the fitted line, the values of j_0 were calculated and are presented in Fig. 7. The exchange current density for the Dy(III)/$Cu_{9/2}Dy$ couple was found to be higher than that for the Dy(III)/Cu_5Dy couple. Fig. 8 shows the plot of ln(j_0) *versus* inverse temperature. The variation of j_0 with temperature was found to follow the Arrhenius law, from which the activation energies associated with the equilibrium reactions were determined. It can be seen that the activation energies for the Dy(III)/Cu_5Dy and Dy(III)/$Cu_{9/2}Dy$ couples are 26.08 kJ mol^{-1} and 22.55 kJ mol^{-1}, respectively. The activation energy for the Dy(III)/Cu_5Dy couple is higher than that for the Dy(III)/$Cu_{9/2}Dy$ couple.

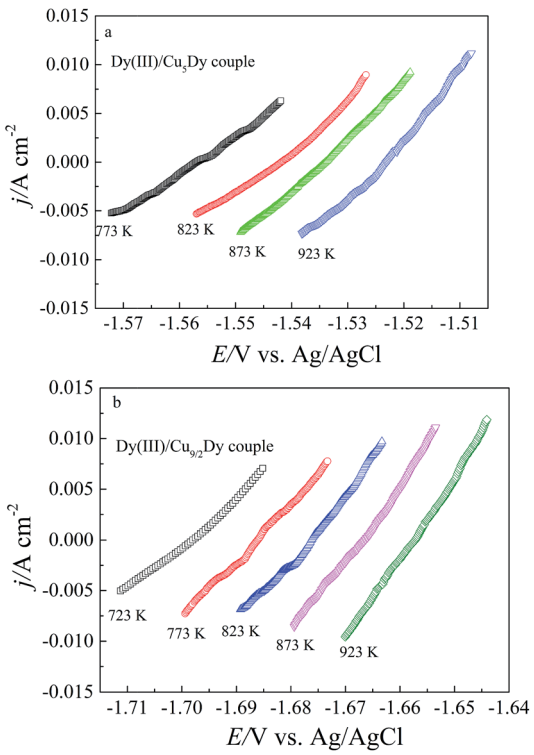

Fig. 6 Cathodic polarization curves by linear polarization of Dy on the Cu cathode in LiCl–KCl eutectic at different polarization potentials.

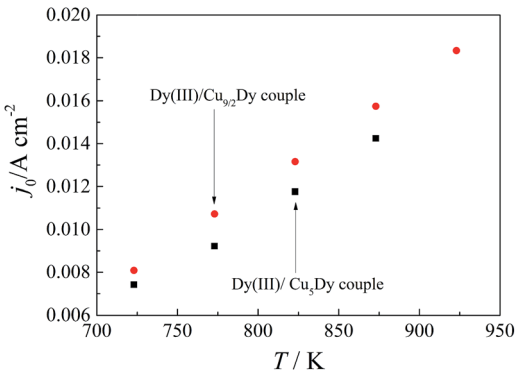

Fig. 7 The values of j_0 for Dy(III)/Cu_5Dy and Dy(III)/$Cu_{9/2}Dy$ couples at different temperatures.

Electroextraction and characterization of Cu–Dy alloys

In order to extract dysprosium and prepare Cu–Dy alloys on the Cu electrode, according to the results of the CV, SWV and OCP

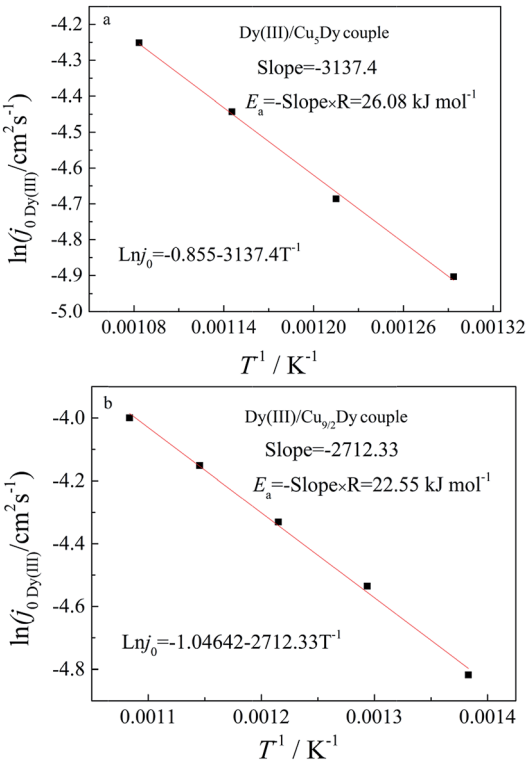

Fig. 8 The change of ln(j_0) *versus* inverse temperature.

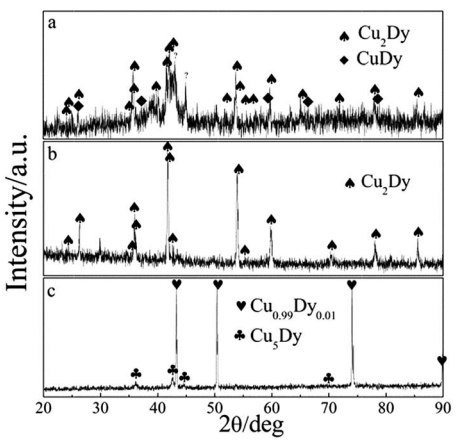

Fig. 9 XRD patterns of the deposits obtained on the Cu electrode (S = 2.15 cm^2) in molten LiCl–KCl–$DyCl_3$ salts for 7 h at 773 K by potentiostatic electrolysis at (a) −2.15 V, (b) −1.77 V and (c) −1.55 V.

(Fig. 2–4), potentiostatic electrolysis was conducted at different potentials on the Cu electrode.

Fig. 9 shows the XRD patterns of extractive productions after potentiostatic electrolysis at −2.15 V (a), −1.77 V (b) and −1.55 V (c) at 773 K on the Cu electrode in LiCl–KCl–$DyCl_3$ (1.34×10^{-4} mol cm^{-3}) melts, respectively. When the potentiostatic electrolysis was performed at −2.15 V, metallic dysprosium is deposited and diffuses into the Cu substrate. Thus, all Cu–Dy intermetallic compounds of the binary system can be expected. However, only two intermetallic compounds Cu_2Dy and CuDy are characterized by XRD analysis (Fig. 9a) in the alloy layer. While when the potentiostatic electrolysis was conducted at −1.77 V, only one Cu–Dy intermetallic compound, Cu_2Dy, is formed. However, at −1.55 V, two intermetallic compounds Cu_5Dy and $Cu_{0.99}Dy_{0.01}$ are prepared. According to the Cu–Dy phase diagram,[40,41] there are four thermodynamically stable Cu–Dy intermetallics (CuDy, Cu_2Dy, $Cu_{9/2}Dy$ and Cu_5Dy) in the system. Since there isn't a $Cu_{0.99}Dy_{0.01}$ phase in the thermodynamically stable phases, we infer that $Cu_{0.99}Dy_{0.01}$ is the metastable phase.

Fig. 10 shows the SEM-EDS of the deposit attained by potentiostatic electrolysis at −2.15 V for 7 h on the Cu electrode at 773 K in the molten LiCl–KCl–$DyCl_3$ (1.34×10^{-4} mol cm^{-3}) salts. The thickness of the deposited layer is approximately

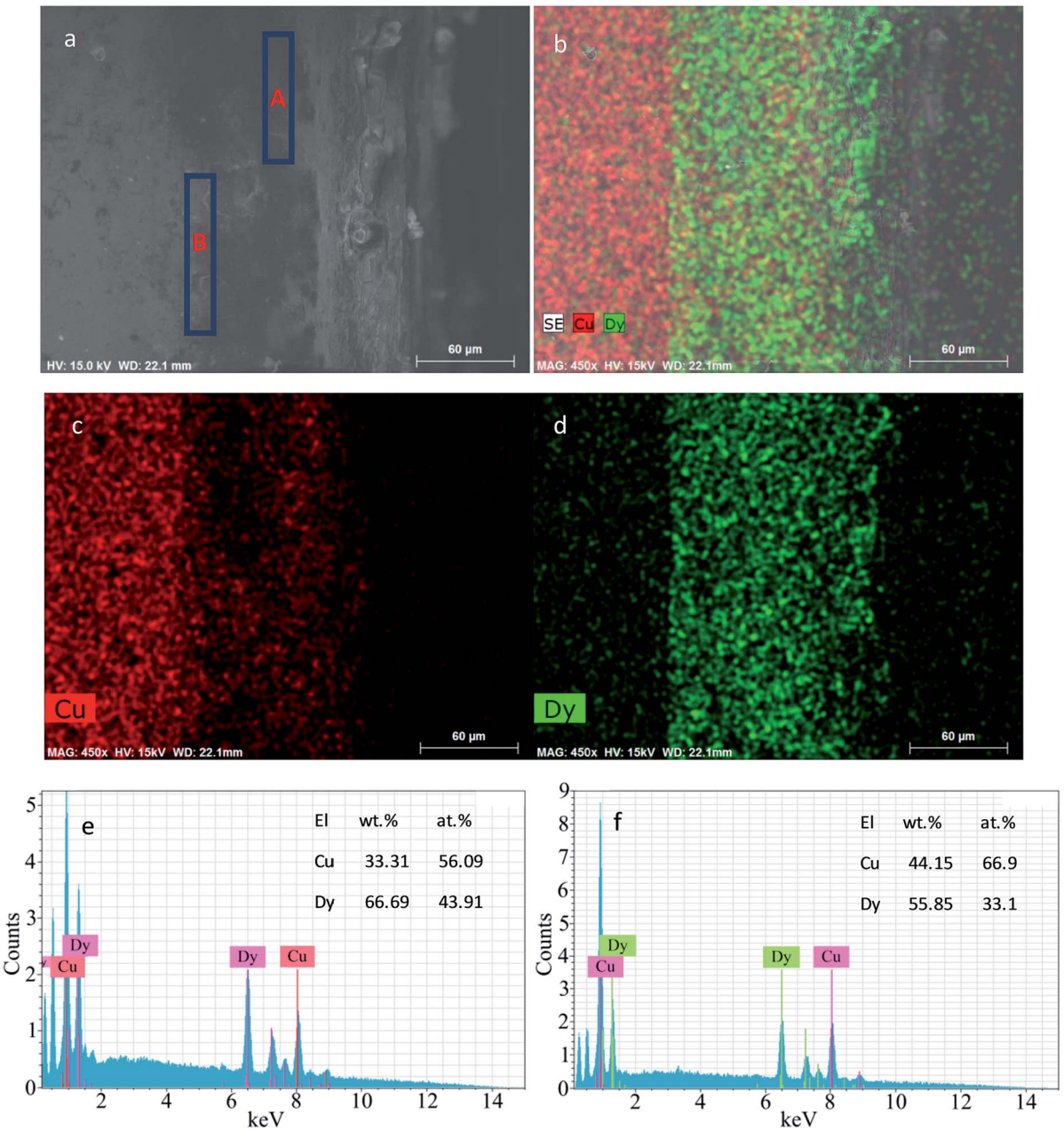

Fig. 10 SEM-EDS of deposit obtained by potentiostatic electrolysis at −2.15 V on the Cu ($S = 2.15$ cm^2) electrode in molten LiCl–KCl–$DyCl_3$ salts for 7 h at 773 K. (a) SEM; (b)–(d) EDS mapping analysis; (e) and (f) EDS point analysis of zones A and B shown in (a).

80 μm (Fig. 10a). As can be seen from the mapping analysis of the elements (Fig. 10b–d), that the deposit mainly consists of Cu and Dy. The atomic ratio of Cu to Dy in zones A and B shown in Fig. 10a are close to 1 : 1 and 2 : 1, respectively (Fig. 10e and f). Combined with the XRD result (Fig. 9a), we think that the alloy layer is comprised of Cu_2Dy and CuDy intermetallic compounds.

Fig. 11 displays the SEM-EDS analysis of the Cu–Dy alloy sample prepared by potentiostatic electrolysis at −1.77 V for 7 h on the Cu electrode at 773 K in the molten LiCl–KCl–$DyCl_3$ (1.34×10^{-4} mol cm^{-3}). The thickness of the alloy layer is about 60 μm (Fig. 11a–c). The atomic ratio of Cu to Dy in zone A shown in Fig. 11a is close to 2 : 1 (Fig. 11d). Combined with the XRD result (Fig. 9b), we infer that the alloy layer consists of the Cu_2Dy intermetallic compound.

Fig. 12 illustrates the SEM-EDS analysis of the Cu–Dy alloy produced by potentiostatic electrolysis at −1.7 V for 7 h on the Cu electrode at 773 K in the molten LiCl–KCl–$DyCl_3$ (1.34×10^{-4} mol cm^{-3}) salts. The thickness of the Cu–Dy alloy layer was about 50 μm. The EDS point analysis labeled A shown in Fig. 12a shows that the Cu/Dy atomic ratio approaches 4.5. The JADE 5.0 software does not provide enough data for parsing the XRD source data obtained from the Cu–Dy sample. However, according to the results of the EDS analysis, we suggested that the deposit layer may consist of the $Cu_{9/2}Dy$ compound (Fig. 11d). Combined with the XRD result (Fig. 9b), we infer that the alloy layer consists of the Cu_2Dy intermetallic compound.

Fig. 13 shows the SEM-EDS of the Cu–Dy alloy produced by potentiostatic electrolysis at −1.55 V for 7 h on the Cu electrode at 773 K. As can be seen from Fig. 13a–c, the thickness of the Cu–Dy alloy layer is about 40 μm. The EDS point analysis labeled zone A reveals that the Cu/Dy atomic ratio is approaching 5.6.

It can be seen from Fig. 10–13, there was an excellent binding force between the Cu–Dy alloy layer and the Cu matrix. Under the same electrolysis conditions, the applied potential can affect the formation of the Cu–Dy compound and the thickness of alloy layer.

Furthermore, the change of the Dy(III) concentration was monitored by ICP-AES during potentiostatic electrolysis at −2.15 V in LiCl–KCl molten salts at 773 K. According to eqn (12), the extraction efficiencies of Dy were evaluated during various electrolysis times.

$$\eta = (C_i - C_f)/C_i \times 100\% \quad (12)$$

where C_i and C_f are the initial and final concentrations of Dy(III) ions in the melts, respectively.

Table 5 list the change of Dy(III) concentrations in the molten salts and extraction efficiencies (η) of Dy metal during the extraction process. As can be seen from Table 5, the

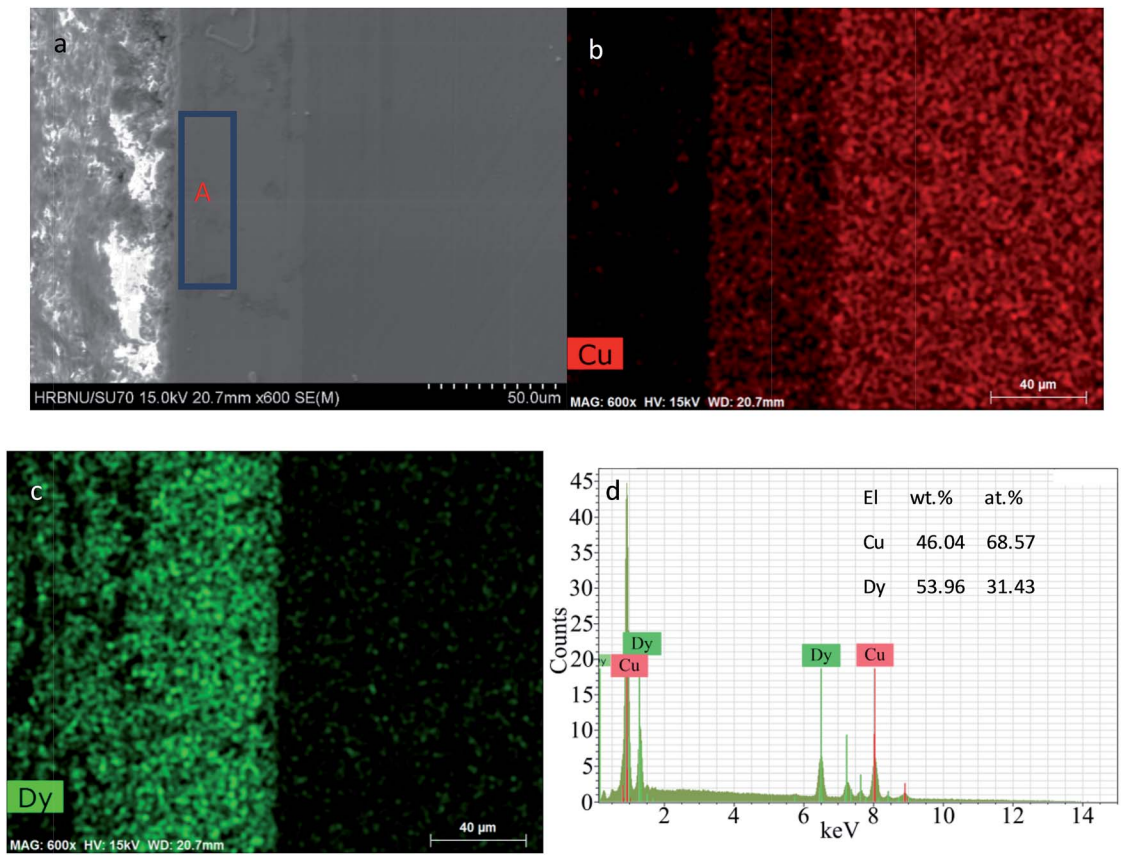

Fig. 11 SEM-EDS of deposit obtained by potentiostatic electrolysis at −1.77 V on the Cu ($S = 2.15$ cm^2) electrode in molten LiCl–KCl–$DyCl_3$ salts for 7 h at 773 K. (a) SEM; (b) and (c) EDS mapping analysis; (d) EDS point analysis of zone A in (a).

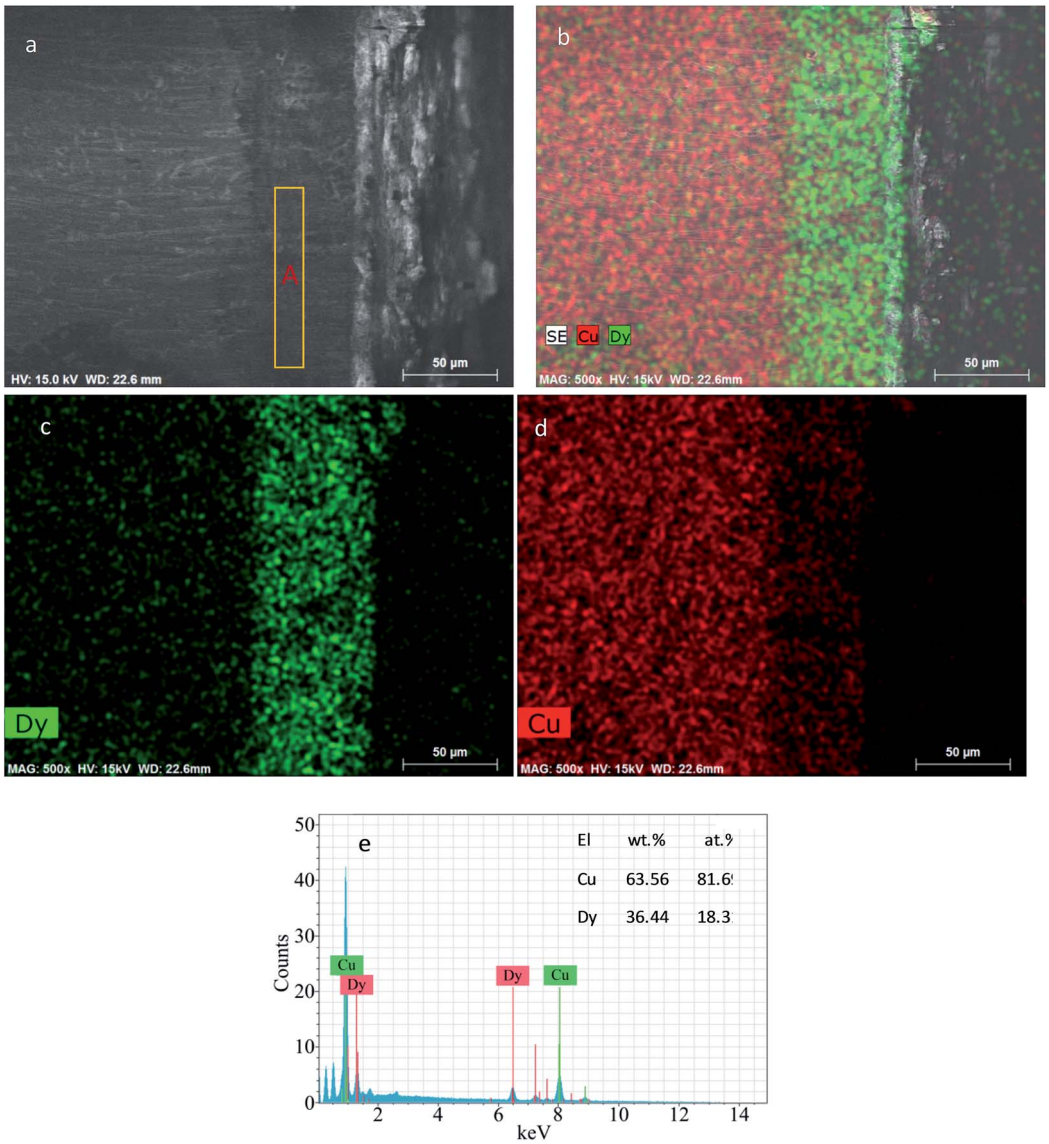

Fig. 12 SEM-EDS of deposit obtained by potentiostatic electrolysis at −1.7 V on the Cu ($S = 2.15$ cm^2) electrode in LiCl–KCl–$DyCl_3$ melts for 7 h at 773 K. (a) SEM; (b)–(d) EDS mapping analyses; (e) EDS point analysis of point A.

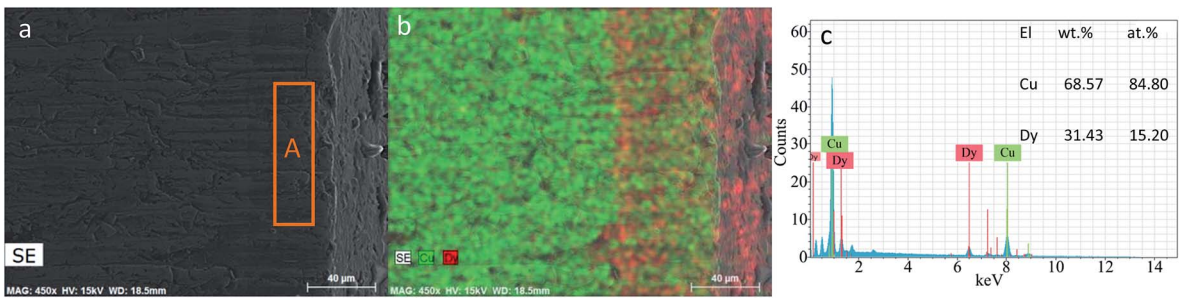

Fig. 13 SEM-EDS of deposit obtained by potentiostatic electrolysis at −1.55 V on the Cu ($S = 2.15$ cm^2) electrode in molten LiCl–KCl–$DyCl_3$ salts for 7 h at 773 K. (a) SEM; (b) EDS mapping analysis; (c) EDS zoned analysis of point A shown in (a).

concentration of Dy(III) in the molten salt decreased from 1.34×10^{-4} mol cm^{-3} to 1.04×10^{-6} mol cm^{-3}. The extraction efficiency of Dy increases with prolonging electrolysis time. The maximum extraction efficiency can reach 99.2% after electrochemical extraction for 16 h. The extraction efficiency of Dy on the Mg electrode from LiCl–KCl–$DyCl_3$ (6.2×10^{-5} mol cm^{-3})

Table 5 The extraction efficiency of dysprosium was calculated using different methods

Extraction time h^{-1}	Concentration of Dy(III) $\times 10^{-4}$/mol cm^{-3}	Mass of Dy on the Cu electrode/g	Extraction efficiency/%	
			ICP-AES	Mass of Dy on the Cu electrode
0	1.340	0	0	0
3	0.805	0.4218	39.9	38.7
8	0.114	0.9341	91.5	85.8
12	0.013	1.0134	99.0	93.1
16	0.011	1.0139	99.2	93.1

melts was calculated to be 98.4% by potentiostatic electrolysis for 24 h at 773 K.[13] Compared with the extraction efficiency of Dy on the Mg electrode, the extraction of Dy on Cu electrode from LiCl–KCl–$DyCl_3$ molten salt is more efficient.

Meanwhile, the increment of Cu electrode was recorded at a different electrolysis time. According to the mass change of the Cu electrode, the extraction quality of the Dy metal was obtained and the extraction efficiency of Dy was also calculated and presented in Table 5. It can be seen from Table 5, there are differences between the extraction efficiencies calculated by the mass change of the working electrode and by ICP-AES. The reason may be that the deposits on the working electrode is physically detached due to harsh condition of electrolysis or large size of the deposit itself, this detached deposit may fall into the molten salts in the form of residue, which reduces the mass of the extraction product. The experimental results indicate that it is effective to extract Dy using Cu as the cathode by potentiostatic electrolysis in molten chlorides.

Conclusion

The electrochemical behavior of Dy(III) was first studied on W in eutectic LiCl–KCl using the electrochemical technique. CV and current reversal chronopotentiogram revealed that the electrochemical reduction of Dy(III) to Dy(0) proceeded in a one-step process involving three electrons. Then, the electrochemical study of Dy(III) on the Cu electrode was carried out in eutectic LiCl–KCl by CV, SWV and OCP. The results of CV and SWV showed that five typical signals correspond to the formation of different Cu–Dy intermetallics. In addition, the standard molar Gibbs free energies, enthalpies, entropies and equilibrium constants of formation for Cu_5Dy, $Cu_{9/2}Dy$, Cu_2Dy and CuDy intermetallics were evaluated by emf measurements in the temperature range of 773–863 K. The j_0 for Dy(III)/Cu_5Dy and Dy(III)/$Cu_{9/2}Dy$ couples were determined by LP. The variation of j_0 with temperature was found to follow the Arrhenius law, from which the activation energies for Dy(III)/Cu_5Dy and Dy(III)/$Cu_{9/2}Dy$ couples were determined and found to be 26.08 kJ mol^{-1} and 22.55 kJ mol^{-1}, respectively. Electrochemical extraction of Dy was performed on the Cu electrode in molten LiCl–KCl–$DyCl_3$ salts at different potentials, and five Cu–Dy compounds, $Cu_{0.99}Dy_{0.01}$, Cu_5Dy, $Cu_{9/2}Dy$, Cu_2Dy and CuDy, were analyzed by XRD and SEM-EDS. The results indicated that applied potential could affect the formation of the Cu–Dy intermetallic compound, and the metastable phase could easily form in molten chlorides on the Cu electrode. The change of the Dy(III) concentration was monitored by ICP-AES during electroextraction at different times and extraction efficiency was calculated. After 16 h electrolysis, the maximum extraction efficiency could reach 99.2%, which indicated that electrochemical extracting Dy on the Cu electrode is feasible from molten chloride.

Conflicts of interest

There are no conflicts to declare.

Acknowledgements

The work was financially supported by the National Natural Science Foundation of China (11575047, 11675044, 21790373, 21271054 and 21173060), the Major Research Plan of the National Natural Science Foundation of China (91326113 and 91226201), National Natural Science Foundation of China (U1630102) and the Fundamental Research Funds for the Central Universities (HEUCFP201790).

References

1 T. Koyama, M. Iizuka, Y. Shoji, R. Fujita, H. Tanaka, T. Kobayashi and M. Tokiwai, *J. Nucl. Sci. Technol.*, 1997, **34**, 384–393.
2 T. H. Pigford, *CA, UCB-NE-4176, Rev. 1*, Department of Nuclear Engineering. University of California at Berkeley, 1990.
3 M. Iizuka, K. Uozumi, T. Inoue, T. Iwai, O. Shirai and Y. Arai, *6th Information Exchange Meeting on Actinide and Fission Product P&T*, Madrid, 2000.
4 J. Uhlíř and M. Mareček, *J. Fluorine Chem.*, 2009, **130**, 89–93.
5 K. Kinoshita, T. Koyama, T. Inoue, M. Ougier and J. P. Glatz, *J. Phys. Chem. Solids*, 2005, **66**, 619–624.
6 G. Y. Kim, D. Yoon, S. Paek, S. H. Kim, T. J. Kim and D. H. Ahn, *J. Electroanal. Chem.*, 2012, **682**, 128–135.
7 O. Conocar, N. Douyere and J. Lacquement, *J. Nucl. Mater.*, 2005, **344**, 136–141.
8 M. Iizuka, T. Koyama, N. Kondo, R. Fujita and H. Tanaka, *J. Nucl. Mater.*, 1997, **247**, 183–190.
9 Y. Castrillejo, A. Vega, M. Vega, P. Hernández, J. A. Rodriguez and E. Barrado, *Electrochim. Acta*, 2014, **118**, 58–66.

10 M. R. Bermejo, E. Barrado, A. M. Martínez and Y. Castrillejo, *J. Electroanal. Chem.*, 2008, **617**, 85–100.
11 M. Li, Q. Q. Gu, W. Han, Y. D. Yan, M. L. Zhang, Y. Sun and W. Q. Shi, *Electrochim. Acta*, 2015, **167**, 139–146.
12 Y. C. Wang, M. Li, W. Han, M. L. Zhang, Y. S. Yang, Y. Sun, Y. C. Zhao and Y. D. Yan, *J. Solid State Electrochem.*, 2015, **19**, 3629–3638.
13 Y. S. Yang, M. L. Zhang, W. Han, P. Y. Sun, B. Liu, H. L. Jiang, T. Jiang, S. M. Peng, M. Li, K. Ye and Y. D. Yan, *Electrochim. Acta*, 2014, **118**, 150–156.
14 X. Li, Y. D. Yan, M. L. Zhang, H. Tang, D. B. Ji, W. Han, Y. Xue and Z. J. Zhang, *Electrochim. Acta*, 2014, **135**, 327–335.
15 T. Iida, T. Nohira and Y. Ito, *Electrochim. Acta*, 2003, **48**, 1531–1536.
16 T. Nohira, H. Kambara, K. Amezawa and Y. Ito, *J. Electrochem. Soc.*, 2005, **152**, C183–C189.
17 M. Li, T. T. Sun, Y. Sun, W. Han and M. L. Zhang, *Acta Phys. - Chim. Sin.*, 2015, **31**, 309–314.
18 P. Chamelot, L. Massot, C. Hamel, C. Nourry and P. Taxil, *J. Nucl. Mater.*, 2007, **360**, 64–74.
19 H. Konishi, T. Nohira and Y. Ito, *Electrochem. Solid-State Lett.*, 2002, **5**, B37–B39.
20 S. Kobayashi, T. Nohira, K. Kobayashi, K. Yasuda, R. Hagiwara, T. Oishi and H. Konishi, *J. Electrochem. Soc.*, 2012, **159**, E193–E197.
21 W. Han, Q. N. Sheng, M. L. Zhang, M. Li, T. T. Sun, Y. C. Liu, K. Ye, Y. D. Yan and Y. C. Wang, *Metall. Mater. Trans. B*, 2013, **45**, 929–935.
22 M. Li, W. Li, W. Han, M. L. Zhang and Y. D. Yan, *Chem. J. Chin. Univ.*, 2014, **35**, 2662–2667.
23 M. Li, T. T. Sun, W. Han, S. S. Wang, M. L. Zhang and Y. D. Yan, *Chin. J. Inorg. Chem.*, 2015, **31**, 177–182.
24 P. Taxil, L. Massot, C. Nourry, M. Gibilaro, P. Chamelot and L. Cassayre, *J. Fluorine Chem.*, 2009, **130**, 94–101.
25 A. Saïla, M. Gibilaro, L. Massot, P. Chamelot, P. Taxil and A. M. Affoune, *J. Electroanal. Chem.*, 2010, **642**, 150–156.
26 C. Nourry, L. Massot, P. Chamelot and P. Taxil, *J. Appl. Electrochem.*, 2008, **39**, 927–933.
27 M. Gibilaro, L. Massot, P. Chamelot, L. Cassayre and P. Taxil, *Electrochim. Acta*, 2009, **55**, 281–287.
28 M. Li, B. Liu, N. Ji, Y. Sun, W. Han, T. Jiang, S. M. Peng, Y. D. Yan and M. L. Zhang, *Electrochim. Acta*, 2016, **193**, 54–62.
29 Y. Wang, M. Li, W. Han, M. L. Zhang, T. Jiang, S. M. Peng and Y. D. Yan, *J. Alloy. Comp.*, 2017, **695**, 3484–3494.
30 Y. Castrillejo, M. R. Bermejo, A. I. Barrado, R. Pardo, E. Barrado and A. M. Martínez, *Electrochim. Acta*, 2005, **50**, 2047–2057.
31 H. Konishi, T. Nohira and Y. Ito, *Electrochim. Acta*, 2002, **47**, 3533–3539.
32 K. Sato, Y. Yosida, Y. Isikawa and K. Mori, *J. Magn. Magn. Mater.*, 1986, **54**, 467–468.
33 S. K. Tripathy, K. G. Suresh, R. Nirmala, A. K. Nigam and S. K. Malik, *Solid State Commun.*, 2005, **134**, 323–327.
34 H. Konishi, T. Nohira and Y. Ito, *J. Electrochem. Soc.*, 2001, **148**, C506–C511.
35 K. Yasuda, S. Kobayashi, T. Nohira and R. Hagiwara, *Electrochim. Acta*, 2013, **106**, 293–300.
36 K. H. Muller, B. Idzikowski, D. Eckert, K. Nenkov, H. J. Engelmann, A. Teresiak and M. Wolf, *IEEE Trans. Magn.*, 1997, **33**, 3565–3567.
37 Z. Wang, J. Ju, J. Wang, W. Yin, R. Chen, M. Li, C. Jin, X. Tang, D. Lee and A. Yan, *Sci. Rep.*, 2016, **6**, 38335.
38 K. Sridharan, S. Martin, M. Mohammadian, J. Sager, T. Allen and M. Simpson, *Trans. Am. Nucl. Soc.*, 2012, **106**, 1240–1241.
39 L. L. Su, K. Liu, Y. L. Liu, L. Wang, L. Y. Yuan, L. Wang, Z. J. Li, X. L. Zhao, Z. F. Chai and W. Q. Shi, *Electrochim. Acta*, 2014, **147**, 87–95.
40 H. Okamoto, *J. Phase Equilibria Diffusion*, 2013, **35**, 195–207.
41 M. Palumbo, L. Battezzati, A. Pasturel, S. G. Schönmeyer and W. Assmus, *Calphad*, 2009, **33**, 511–516.
42 Y. Castrillejo, C. Abejbn, M. Vega and R. Pardo, *Electrochim. Acta*, 1997, **42**, 1495–1506.
43 F. Sommer, J. Schott and B. Predel, *J. Less Common Met.*, 1986, **125**, 175–181.
44 A. J. Bard and L. R. Faulkner, Electrochemical Methods, *Fundamental and Applications*, Wiley, New York, 2001, p. 308.